Super-Resolution Imaging of C-Type Lectin and Influenza Hemagglutinin Nanodomains on Plasma Membranes Using Blink Microscopy

Michelle S. Itano,[†] Christian Steinhauer,[‡] Jürgen J. Schmied,[‡] Carsten Forthmann,[‡] Ping Liu,[†] Aaron K. Neumann,[†§] Nancy L. Thompson,[¶Δ] Philip Tinnefeld,[‡Δ] and Ken Jacobson[†§Δ*]

[†]Department of Cell and Developmental Biology, University of North Carolina at Chapel Hill, Chapel Hill, North Carolina; [‡]Physikalische und Theoretische Chemie-NanoBioSciences, Braunschweig University of Technology, Braunschweig, Germany, and Center for NanoScience, Munich, Germany; and [§]Lineberger Comprehensive Cancer Center and [¶]Department of Chemistry, University of North Carolina at Chapel Hill, Chapel Hill, North Carolina

ABSTRACT   Dendritic cells express DC-SIGN, a C-type lectin (CTL) that binds a variety of pathogens and facilitates their uptake for subsequent antigen presentation. DC-SIGN forms remarkably stable microdomains on the plasma membrane. However, inner leaflet lipid markers are able to diffuse through these microdomains suggesting that, rather than being densely packed with DC-SIGN proteins, an elemental substructure exists. Therefore, a super-resolution imaging technique, Blink Microscopy (Blink), was applied to further investigate the lateral distribution of DC-SIGN. Blink indicates that DC-SIGN, another CTL (CD206), and influenza hemagglutinin (HA) are all localized in small (~80 nm in diameter) nanodomains. DC-SIGN and CD206 nanodomains are randomly distributed on the plasma membrane, whereas HA nanodomains cluster on length scales up to several microns. We estimate, as a lower limit, that DC-SIGN and HA nanodomains contain on average two tetramers or two trimers, respectively, whereas CD206 is often nonoligomerized. Two-color Blink determined that different CTLs rarely occupy the same nanodomain, although they appear colocalized using wide-field microscopy. What to our knowledge is a novel domain structure emerges in which elemental nanodomains, potentially capable of binding viruses, are organized in a random fashion; evidently, these nanodomains can be clustered into larger microdomains that act as receptor platforms for larger pathogens like yeasts.

INTRODUCTION

Immature dendritic cells are professional antigen presenting cells that mediate innate and adaptive immune responses by first detecting and binding to a large variety of pathogens (1,2). This antigen recognition is driven by interactions of pathogens with specialized receptors, highly expressed on the surface of dendritic cells that recognize pathogen-associated molecular patterns. C-type lectins (CTLs) are one such family of receptors that recognize carbohydrate epitopes on the surface of many pathogens (3). One CTL, DC-SIGN (dendritic cell-specific intercellular adhesion molecule-3-grabbing nonintegrin), also called CD209, is a type II membrane protein that binds to a large range of clinically relevant pathogens, including HIV, Ebola virus, *Candida albicans*, and *Leishmania* (4). DC-SIGN is expressed in microdomains on the surfaces of dendritic cells and when ectopically expressed in fibroblasts and other cell types (5–9). Furthermore, in vitro studies indicate that DC-SIGN is most probably present as a tetramer on the plasma membrane (10–16). Recognition of and binding to pathogens by DC-SIGN appears to require that the

presumed DC-SIGN tetramers, or at least DC-SIGN as a monomer, be clustered on the plasma membrane (5).

DC-SIGN forms clusters on the cell surface even in the absence of exogenous ligands and these clusters enable DC-SIGN to bind to pathogens ranging in size from viruses (typically 80–100 nm in diameter) to yeast particles (several microns in diameter). In fact, previous measurements using wide-field microscopy methods have indicated that DC-SIGN microdomains both on human immature dendritic cells and on fibroblasts ectopically expressing DC-SIGN range in size from that detectable by classical optical resolution ($\approx$300 nm) to ~1.5 μm in dimension (8). Other work, using transmission electron microscopy (TEM) and near-field scanning optical microscopy (NSOM), has indicated that DC-SIGN clusters are generally <200 nm in diameter (5–7). Recent results using several complementary fluorescence imaging-based techniques to measure the lateral dynamics of DC-SIGN microdomains indicated that these microdomains are remarkably stable (8,9). However, fluorescence recovery after photobleaching experiments determined that lipids can permeate and diffuse through DC-SIGN microdomains (9), suggesting that, rather than being densely packed with DC-SIGN proteins, there may be a complex internal structure to DC-SIGN microdomains that are viewed as continuous structures using wide-field fluorescence microscopy. Throughout this work, we will refer to domains observable by wide-field fluorescence microscopy, having a resolution limit of ~300 nm, as microdomains, whereas domain structures with dimension

*Correspondence: frap@med.unc.edu

Aaron K. Neumann's present address is Department of Pathology, University of New Mexico School of Medicine, Albuquerque, NM.

Editor: Petra Schwille.

~100 nm or less, which are only observable by super-resolution methods, will be referred to as nanodomains.

The studies reported in this work describe results obtained by using a super-resolution imaging technique, Blink Microscopy (Blink), to examine the nanostructure of DC-SIGN microdomains on fixed dendritic cells. Blink is one of several recently developed methods that use sequential, sparsely distributed single-molecule imaging to generate plots of precise locations of single molecules, with a resolution of ~30 nm (17). This method employs oxidation and reduction agents to drive the majority of the dyes into transient dark states, with only a few sparsely distributed dyes fluorescing, with ms-long on times, at a time. Blink offers several advantages for biological applications because it permits the use of commercial dyes (and therefore doesn't require overexpression of a fluorescent protein fusion), it uses fast (<120 s) times for image acquisition (2–4000 frames at 30 ms integration times), and is experimentally simple to setup (requiring only the use of standard immunostaining practices and the exchange of soluble buffers). However, as with many of the other super-resolution imaging methods, Blink is most effective when imaging fixed cells using total internal reflection fluorescence (TIRF) microscopy, and therefore can be most easily applied to image proteins at or very near the ventral cell surface or coverslip.

For comparative purposes, the distribution of DC-SIGN at suboptical resolution was complemented by observations of another protein, influenza hemagglutinin (HA). HA is located in the viral envelope, but also forms plasma membrane microdomains when ectopically expressed in noninfected cells. The propensity for HA to form microdomains on plasma membranes is presumably related to subsequent viral budding (18,19). Analysis of Blink images determined that DC-SIGN and HA are predominantly expressed in small nanodomains, ~80 nm in diameter. However, although statistical analyses showed that DC-SIGN nanodomains are randomly distributed on dendritic cell surfaces, the same analyses indicated that HA nanodomains are not randomly distributed on NIH 3T3 HAb2 cell surfaces at length scales up to and beyond 1 μm. Finally, the number of Blink localizations per nanodomain indicated that DC-SIGN and HA nanodomains generally contain fewer than 12 molecules, suggesting that these nanodomains are not densely packed with DC-SIGN or HA molecules, respectively, leaving room for other protein and lipid components.

To determine whether the spatial arrangement of DC-SIGN is representative of other members of the CTL family of proteins, Blink was applied to investigate the lateral distribution of another CTL family member, CD206. Analysis of Blink images indicated that, similar to DC-SIGN, CD206 is also generally expressed in randomly distributed, small (<80 nm in diameter) nanodomains. However, CD206 nanodomains appear to contain fewer molecules on average than DC-SIGN and HA nanodomains. Furthermore, two-color Blink imaging determined that

different CTLs (DC-SIGN and CD206) are generally confined to separate nanodomains and rarely coexists within the same nanodomain, though when viewed by wide-field microscopy they appear to be colocalized.

Overall, the results reported here indicate that there is a lateral organization of nanodomains within DC-SIGN and CD206 microdomains, which cannot be resolved by wide-field fluorescence microscopy; give a considerable amount of quantitative insight with respect to this complexity; and raise key questions concerning structure-function relationships for certain classes of membrane receptor clusters.

MATERIALS AND METHODS

Due to space constraints, this section is described in full detail in the Supporting Material.

RESULTS

Blink on DC-SIGN plasma membrane nanodomains

DC-SIGN forms remarkably stable microdomains on the plasma membrane that range in size, as estimated from wide-field fluorescence microscopy, from the diffraction limit to ~1.5 μm in dimension (8,9). However, inner leaflet lipid markers are able to diffuse through these microdomains suggesting that rather than being densely packed with DC-SIGN proteins, an elemental substructure exists (9). Therefore, a super-resolution imaging technique, Blink (17), was applied to further investigate the lateral distribution of DC-SIGN within microdomains on the plasma membrane. Blink achieves subdiffraction limited resolution by precisely localizing single molecules that are stochastically imaged in a sequential manner so that no more than one molecule is actively emitting fluorescence within the point spread function of the molecule (20).

Before antibody staining and imaging, all cells were fixed by using a paraformaldehyde solution (4% (w/v) in phosphate buffered saline (PBS), pH 7.4) for 20 min at 25°C and then maintained in 0.1% (w/v) bovine serum albumin in PBS overnight at 4°C. Fixed monocyte-derived immature dendritic cells were stained for DC-SIGN using indirect immunofluorescence with DC6 IgG and ATTO655-Fab. Blink images were generated from movies taken while the dyes were induced to blink with ms-long on-times in the presence of reducing and oxidizing agents. Specifically, cells labeled with primary and secondary antibodies were imaged in PBS containing both 50–100 μM ascorbic acid and 0–75 μM N,N-methylviologen. Ascorbic acid and N,N-methylviologen concentrations were adjusted to gain sufficient localizations within 120 s. Each point in a Blink image represents the precise location of a single molecule given by fitting the spatial distribution of the fluorescence from a single molecule to a Gaussian function. Fig. 1 shows
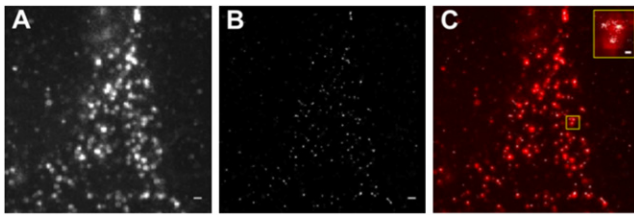
FIGURE 1 Blink on DC-SIGN plasma membrane nanodomains. (*A*) Image of DC-SIGN expression on a fixed dendritic cell stained with DC6 and anti-mouse ATTO655-Fab using diffraction limited TIRF illumination. (*B*) Super-resolution Blink image of DC-SIGN expression of the same region in *A*. (*C*) Overlay of TIRF image (in *red*) and Blink image (in *white*). Scale bars, 500 nm; scale bar inset, 100 nm.

a representative image (one of 17 images analyzed): Fig. 1 *A* gives the conventional TIRF image; Fig. 1 *B* gives the Blink image; and Fig. 1 *C* gives an overlay of the Blink image and the TIRF image. It can be readily seen by comparing Fig. 1, *A* and *B*, Blink provides a much higher resolution in terms of localizing centroids of DC-SIGN micro/nanodomains in the same region of the cell. For example, in some cases where a single region of fluorescence or microdomain is viewed using TIRF, the Blink image indicates that this area is actually composed of several very small nanodomains (Fig. 1 *C*, *inset*). Additionally, the TIRF image (Fig. 1 *A*) and the corresponding computer-generated convolution of the Blink image to a corresponding wide-field image (Fig. S1 in the Supporting Material) are very similar. Nonetheless, these two images are not completely identical. Most of the variation is due to differences in relative pixel intensity values between the two images, because the values in Fig. 1 *A* reflect actual fluorescence intensities, whereas the values in Fig. S1 were generated computationally. In addition, the number of Blink localizations within a pixel area should be, for the most part, correlated with the number of fluorophores in the area, but will also depend on the specific

blinking properties during the imaging conditions (e.g., how long given fluorophores were in the on-state), possible differences in photobleaching, and the likelihood that more than one fluorophore within the point spread function at a given location is in an on-state at the same time. Furthermore, there are some areas in the TIRF image (*A*) that do not appear in either the Blink image (*B*) or the Blink image following convolution (Fig. S1); most likely because the TIRF image is taken at the beginning of the movie (when all fluorophores are in the on-state), but subsequently some of the fluorophores irreversibly photobleach and are not able to be detected by Blink.

Size estimation of DC-SIGN plasma membrane nanodomains using Blink

Blink images of DC-SIGN on fixed dendritic cells stained with DC6 and anti-mouse ATTO655-Fab allowed visualization of small DC-SIGN nanodomains on the plasma membrane. To determine the range in sizes of these nanodomains, the Blink images were analyzed using ImageJ and custom-built Labview software. Nanodomains were first identified using the Particle Analyzer routine in ImageJ (Fig. 2). The spatial distributions of Blink localizations in each nanodomain were then fit to two-dimensional Gaussian functions and the full width at half-maximum (FWHM) values, of the fitted Gaussian functions, were used to estimate nanodomain diameters (Fig. 2). The average FWHM for DC-SIGN nanodomains was 76 ± 42 nm (mean ± standard deviation for 3706 FWHM measurements, derived from 1853 nanodomains on 17 cells; Table 1 and Fig. 3). It is notable that the majority of the DC-SIGN nanodomains are smaller than 100 nm in diameter (Fig. 3), which is significantly less than the ~500 nm microdomain dimension observed in TIRF and epifluorescence images (Fig. 1 *A* and (8)). These results are consistent
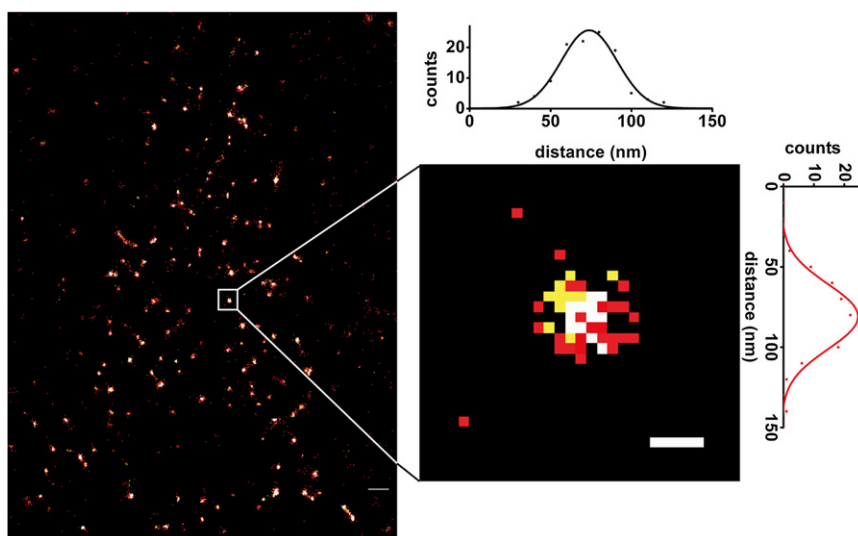

FIGURE 2 Determining DC-SIGN nanodomain size using Blink. Super-resolution Blink image of DC-SIGN expression on a fixed dendritic cell stained with DC6 and anti-mouse ATTO655-Fab. The density of Blink localizations is denoted with black being least dense and white being most dense. Scale bar, 500 nm. A close-up view of the Blink localizations in a single DC-SIGN nanodomain, highlighted in the white box, appears to the right of the original image (scale bar, 50 nm). A graph showing the distribution of the Blink localizations in the nanodomain in the *x* dimension appears above the Blink image of the single nanodomain, and the Gaussian fit along the *x* axis is shown with the black line. The data in the *y* dimension are depicted in the graph in a vertical orientation to the right of the Blink image of the single nanodomain, and the Gaussian fit along the *y* axis is shown with the red line.

TABLE 1 Characteristics of DC-SIGN, CD206, and HA nanodomains as measured by Blink Microscopy

	DC-SIGN domains			CD206 domains		
	Mean (median)	Range	n (m)	Mean (median)	Range	n (m)
Overall FWHM (nm)	76 ± 42 (66)	20–991	3706 (17)	70 ± 41 (59)	17–300	2819 (13)
Area (nm^2)	5100 ± 6100 (3300)	670–80814	1853 (17)	4400 ± 4700 (2800)	360–45247	1409 (13)
Number of Blink localizations	163 ± 230 (82)	8–2283	1960 (17)	78 ± 168 (24)	5–2357	1409 (13)

	HA domains			Single ATTO655-Fabs		
	Mean (median)	Range	n (m)	Mean (median)	Range	n (m)
Overall FWHM (nm)	74 ± 47 (61)	24–486	2910 (12)	39 ± 11 (38)	24–91	191 (6)
Area (nm^2)	5200 ± 7800 (2900)	559–90554	1455 (12)	1200 ± 580 (1200)	553–3285	97 (6)
Number of Blink localizations	120 ± 142 (71)	11–1688	1099 (12)	25 ± 18 (22)	5–111	97 (6)

Uncertainties are standard deviations. Parameters m and n are the numbers of images and nanodomains analyzed, respectively.

with those from other studies using methods with high spatial resolution, TEM and NSOM, which have also determined that DC-SIGN is predominantly localized in domains <200 nm in diameter (5–7). However, the DC-SIGN nanodomains imaged by Blink are slightly smaller on average than those that were previously analyzed using these other techniques. For the NSOM measurements, the average DC-SIGN domain size (~100 nm) was at the lower limit of spatial resolution for this method (90–100 nm). Furthermore, the relatively large (10 nm) gold particles used for labeling antibodies for the TEM experiments may have resulted in slightly larger domain size measurements.

Comparison of size estimation of DC-SIGN plasma membrane nanodomains to those of influenza HA and CD206, another C-type lectin, using Blink

Although the results presented thus far have primarily focused on describing the spatial distribution of DC-SIGN, work focused on describing heterogeneity on the plasma membrane and the downstream consequences of such molecular assemblies has become an issue of considerable interest. Influenza HA domains, when HA is ectopically expressed, have been investigated by different imaging modalities (21,22), and, therefore, it is useful to compare our results from DC-SIGN to those from HA. HA is a glycoprotein that is expressed on the envelope of influenza viruses and is required for the virus to bind to and be internalized either by target cells for infection or by immunological cells for antiviral immunity (23). On virally infected cells, HA assembles into plasma membrane domains, presumably at sites of subsequent viral budding from the cell surface (18,19). When HA is ectopically expressed in fibroblasts, without other viral proteins, HA appears to accumulate into domains (ranging from 30 nm to several microns in diameter) on the plasma membrane of fixed and live cells (18,21,22). Consistent with these previous findings, Blink on fixed HAb2 cells, a NIH 3T3

cell line that stably expresses HA, indicates that the protein is distributed in clusters on the cell surface. The size distribution of these clusters was analyzed using the same method described previously for DC-SIGN. Similar to the distribution of DC-SIGN, HA is expressed in small nanodomains, the majority of which are <100 nm in diameter (2910 FWHM measurements derived from 1455 nanodomains on 12 cells; Table 1 and Fig. 3). These nanodomains of HA were similar in dimension to the compact clusters described by Hess et al. (21); however, because our analysis did not include the cell borders, we did not analyze the elongated clusters observed earlier.

Additionally it is useful to compare the clustering of DC-SIGN to that of another CTL family member, CD206, to investigate whether the spatial arrangement of DC-SIGN is representative of other members of the CTL family of proteins. Previously, it was determined that CD206 was also expressed in microdomains on the plasma membrane
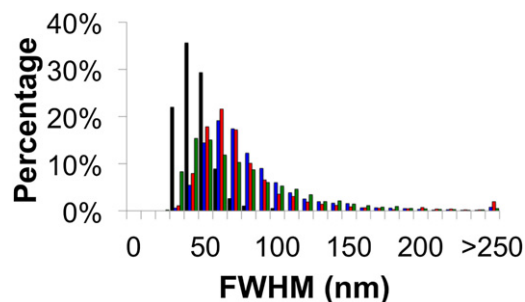

FIGURE 3 Size estimation of DC-SIGN, CD206, and HA plasma membrane nanodomains using Blink. FWHM values obtained by Blink of single ATTO655-Fab molecules (*black bars*), DC-SIGN nanodomains on dendritic cells stained with DC6 and anti-mouse ATTO655-Fab (*blue bars*), CD206 nanodomains on dendritic cells stained with AF2534 and anti-goat ATTO655-Fab (*green bars*), and HA nanodomains on HAb2 cells stained with FC125 and anti-mouse ATTO655-Fab (*red bars*). As shown, DC-SIGN, CD206, and HA nanodomains all have similar size distributions. The average nanodomain size is much larger than the spatial accuracy of the method as determined by imaging single ATTO655-Fab molecules and is much smaller than the conventional wide-field fluorescence microscopy resolution limit.

of dendritic cells, and that these microdomains sometimes colocalized with DC-SIGN microdomains (9). Blink on fixed dendritic cells stained with AF2534 and anti-goat ATTO655-Fab determined that CD206 is also expressed in nanodomains, which are 70 ± 41 nm in diameter (2819 FWHM measurements, derived from 1409 nanodomains on 13 cells; Table 1 and Fig. 3). This result suggests that other CTLs may also have distinct nanoscale architecture.

Estimated localization precision of Blink by imaging single ATTO655-Fab molecules on glass

Similar to other super-resolution imaging techniques that use stochastic activation of fluorophores, each dye imaged by Blink is typically localized multiple times (fit to Gaussian functions in multiple frames) in the final Blink image. Therefore, although the localization precision of a single dye in a single frame depends on the number of photons collected (24), the localization precision of a single dye in a Blink image is also related to the spatial distribution of all of the Blink localizations derived from a single dye. To determine localization precision including the influence of multiple localizations of single dyes, Blink images of sparsely distributed single anti-mouse ATTO655-Fab molecules on glass were analyzed. Based on the number of bleaching steps for many individual ATTO655-Fabs, the average dye/protein ratio was determined to be 1.4 (Fig. S2). The average FWHM of the Gaussian fits to the distributions of Blink localizations from single ATTO655-Fabs on glass was 39 ± 11 nm (191 FWHM measurements, 97 dyes; Table 1). It is notable that the average FWHM measurements for DC-SIGN and HA nanodomains are significantly larger than the localization precision for a single fluorescent Fab (Fig. 3); therefore, it is highly unlikely that the FWHM measurements of DC-SIGN are of single Fabs, and much more likely that the FWHM measurements refer to the dimensions of DC-SIGN nanodomains on the plasma membrane.

DC-SIGN and CD206, but not HA, nanodomains are randomly distributed on the plasma membrane

Blink provides high-resolution spatial distribution data, which allows mapping of the precise locations (or centroids) of nanodomains and makes possible discrimination between whether DC-SIGN and CD206 nanodomains are randomly or nonrandomly distributed on the cell surface. Using the PAST (25) and the Cellspan (26) analysis programs, Ripley's K and modified Hopkin's tests were applied to the distributions of nanodomain centroids from Blink images that were cropped to exclude cell boundaries and areas not covered by a cell, respectively. In the case of the Ripley's K test, the PAST program was used to calculate the function $K(r)$, which indicates the probability of encoun-

tering another centroid at the length scale denoted on the r axis. For random distributions the function $K(r)$ is proportional to the density of the centroids and πr^2. Red lines in the plots (Fig. 4, C, F, I) represent the 95% confidence interval for complete spatial randomness calculated from 1000 Monte Carlo simulations of randomly distributed points for each image. Clustering is indicated at length scales where $K(r)$ is greater than that expected due to a random distribution of points. Cellspan's modified Hopkin's test for spatial randomness compares the distances between random data points and nanodomain centroids to the actual distances between nanodomain centroids. A random distribution is indicated by a function that is shaped like a normal bell curve centered at the Hopkin's statistic 0.5 on the abscissa. Clustering is indicated if the plot is shifted to the right. For both of these analyses, the distribution of DC-SIGN and CD206 nanodomain centroids aligns closely with the expected result for a random distribution (Fig. 4, A–F). This finding agrees with the NSOM data (6).

Very different results were obtained when the same analysis methods were applied to centroids derived from Blink images of HA (Fig. 4, G–I). For every HA image analyzed (12 of 12 images), the modified Hopkin's test indicated clustering and the Ripley's K test indicated clustering of multiple nanodomains across all length scales up to 1 μm. For the Ripley's K test, clustering is indicated by the $K(r)$ statistic being greater than the value expected for a random distribution at the length scales indicated by the values on the abscissa. The $K(r)$ statistic for HA nanodomain centroids was consistently greater than the parabolic curve expected for a random distribution from the shortest distances measureable (~30 nm) to >1 μm. In many cases, the Ripley's K test indicated clustering for even longer distances. These results are consistent with previous analysis of the distribution of HA using electron microscopy and fluorescence photoactivation localization microscopy (21). These results also indicate that the assembly and/or the maintenance of DC-SIGN and CD206 nanodomain distributions on the cell surface are regulated by distinct mechanisms from those that occur with HA nanodomains.

Estimated occupancy of DC-SIGN in single nanodomains using Blink

Because the number of Blink localizations in a DC-SIGN nanodomain is, on the average, proportional to the number of molecules in the nanodomain, it is possible to estimate the occupancy of DC-SIGN in nanodomains using data derived from Blink images of DC-SIGN on fixed dendritic cells. A single molecule, in this case a single Fab, will blink with a characteristic rate, leading to an average number of Blink localizations that will be derived from a single Fab imaged with consistent experimental conditions. The average number of Blink localizations from a single Fab
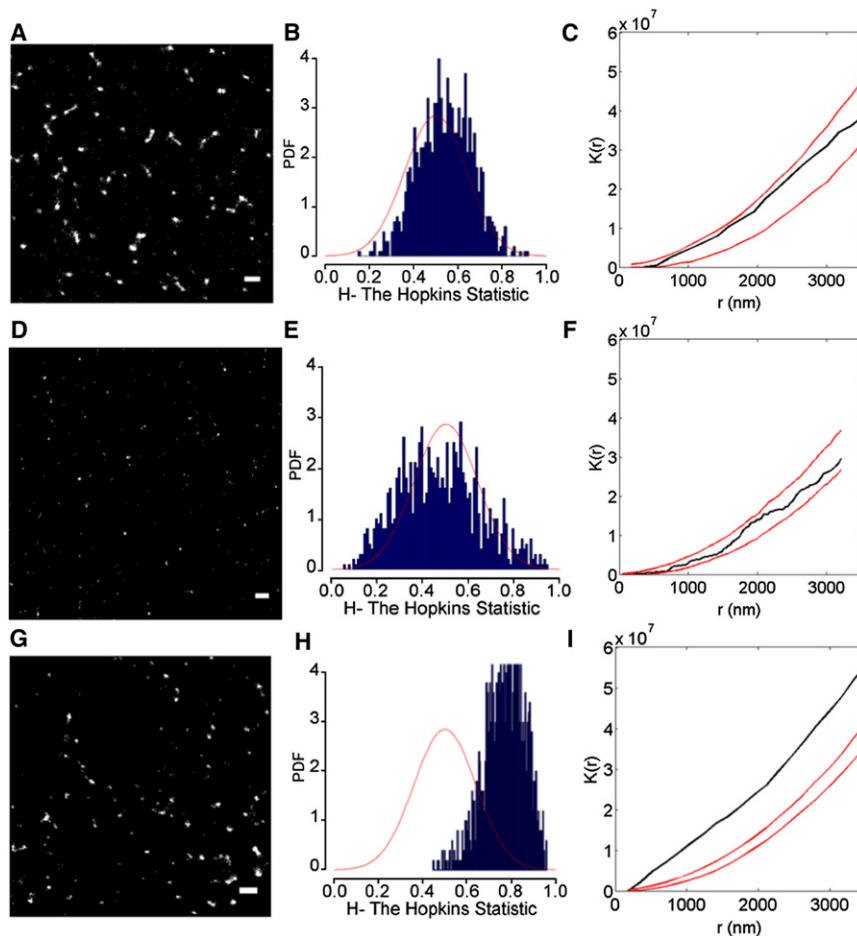
FIGURE 4 DC-SIGN and CD206, but not HA, nanodomains are randomly distributed on the plasma membrane. (*A, D* and *G*) Binarized super-resolution Blink images (cropped to exclude cell borders) of DC-SIGN expression on dendritic cells stained with DC6 and anti-mouse ATTO655-Fab (*A*), of CD206 expression on dendritic cells stained with AF2534 and anti-goat ATTO655-Fab (*D*), or of HA expression on HAb2 cells stained with FC125 and anti-mouse ATTO655-Fab (*G*); these images are representative of a collection of 16, 13, and 12 analyzed for DC-SIGN, CD206, and HA, respectively. (*B, E,* and *H*) Results of a modified Hopkin's test for spatial randomness on centroids of DC-SIGN (*B*), CD206 (*E*), or HA (*H*) nanodomains (in *blue*) from the images in *A, D,* and *G,* respectively. The distribution expected if the centroids were distributed randomly is depicted with the red lines. A nonrandom distribution or clustering would be indicated by a shift in the distribution to the right. (*C, F,* and *I*) Results from a Ripley's K test for spatial randomness on centroids of DC-SIGN (*C*), CD206 (*F*), or HA (*I*) nanodomains (*black lines*) from the images in *A, D,* and *G,* respectively. The red lines indicate the 95% confidence interval for complete spatial randomness calculated from 1000 Monte Carlo simulations of random distributions of centroids. Scale bars, 500 nm.

was 25 ± 18 (97 dyes analyzed; Table 1, Fig. 5 *A*). There is variability in the number of Blink localizations from single Fabs as different molecules may have zero, one, two, or perhaps even three conjugated fluorophores (Fig. S2). In addition, the blinking of each dye is a stochastic process sometimes leading to the dye having slightly longer or shorter on-times during the imaging process, leading to more or fewer blink localizations per single dye in a given blink image. Using the same laser power, camera integration time, concentrations of antibodies, and analysis conditions, the average number of Blink localizations from a single DC-SIGN nanodomain was found to be 163 ± 230 (1960 nanodomains analyzed; Table 1, Fig. 5 *A*). As shown in Fig. 5 *A* and indicated by the large standard deviation of the measurement, there is a large variability in the number of Blink localizations from single DC-SIGN nanodomains. The total number of Blink localizations in a single nanodomain is equal to the sum of Blink localizations from all of the single molecules in the nanodomain. Therefore, an estimate of the occupancy of DC-SIGN in single nanodomains was calculated by dividing the number of Blink localizations in a single nanodomain by the average number of Blink localizations from a single dye. The majority of both DC-SIGN and HA nanodomains contain fewer than

12 molecules (7 ± 10 and 5 ± 6, 1960 and 1099 nanodomains analyzed, respectively) with a few nanodomains (<100 nm in diameter) of each type accommodating upward
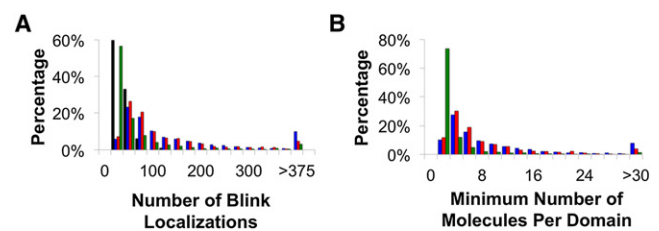

FIGURE 5 Estimated occupancy of DC-SIGN, CD206, and HA in single nanodomains using Blink. (*A*) Histogram of the number of Blink localizations for single ATTO655-Fab antibodies on glass (*black bars*), single DC-SIGN nanodomains on dendritic cells stained with DC6 and anti-mouse ATTO655-Fab (*blue bars*), CD206 nanodomains on dendritic cells stained with AF2534 and anti-goat ATTO655-Fab (*green bars*), and HA nanodomains on HAb2 cells stained with FC125 and anti-mouse ATTO655-Fab (*red bars*). (*B*) Histogram of the minimum number of DC-SIGN molecules per nanodomain on dendritic cells (*blue bars*), of CD206 molecules per nanodomain on dendritic cells (*green bars*), and of HA molecules per nanodomain on HAb2 cells (*red bars*). Minimal occupancies for each nanodomain type were determined by dividing the number of Blink localizations per nanodomain by the average number of Blink localizations for a single Fab on glass.

of ~65 molecules (Table 1, Fig. 5 A). CD206 nanodomains, on the other hand, appear to contain fewer molecules on average, with a larger population of what appear to be single, nonoligomerized molecules on the cell surface (1409 nanodomains analyzed; Table 1, Fig. 5 A). Given the average diameter of the ectodomain of a tetramer of DC-SIGN of ~8 nm (27,28), we calculated that ~360 molecules of DC-SIGN or ~90 tetramers could fit within a nanodomain of average size (~76 nm in diameter; Table 1). However, we regard the nanodomain occupancy estimate as a lower limit for the following reasons: 1), a portion of the population of labeling Fabs will bind but have no dye conjugated to them; 2), whether, at saturation binding conditions for the primary antibody, every DC-SIGN can be labeled due to steric hindrance between adjacent binding antibodies; and 3), whether one bivalent primary antibody can bind two proximate DC-SIGN molecules. Nevertheless, even if the average number of DC-SIGN molecules in nanodomains was underestimated by a factor of two to three, the nanodomain would not be fully occupied by close packed DC-SIGN proteins (see Fig. 7).

DC-SIGN does not significantly colocalize with CD206 on the nanoscale

Wide-field fluorescence microscopy indicates that in a significant fraction of cases, Dectin-1 or CD206 colocalize with DC-SIGN on the resolution level of the light microscope (9). Whether this result holds on the nanoscale has important implications for membrane function. It is likely that whether CTLs are separated into different elemental nanodomains and/or co-mingled in the same nanodomain will regulate their downstream signaling (i.e., either by segregating downstream enzymes and substrates or by providing coincidence of two pathways both impinging on common downstream targets). Two-color Blink using ATTO655 and Alexa546 to label the two different secondary antibodies was applied to test whether DC-SIGN and CD206 are colocalized on the nanoscale (Fig. 6, Fig. S3). To optimize the blinking of both fluorophores for two-color measurements, some cells were imaged in an alternative solution that achieved oxygen removal enzymatically (2% glucose in PBS with 50 μg/ml glucose oxidase, 100–200 μg/ml catalase, 0.1 mM TCEP-HCl (Sigma, Deisenhofen, Germany), and contained 1–50 mM cysteamine (MEA, Sigma) as a reducing agent. Approximately the same % colocalization is calculated for both the two-color Blink images (20 images analyzed) and for simulated images (100 images analyzed) of two overlapping randomly distributed sets of nanodomains (3.4 ± 1.9 and 1.9 ± 0.1%, respectively, Fig. S3). This super-resolution imaging determined that these two different CTLs are generally confined to separate nanodomains, and rarely coexist within the same nanodomain.
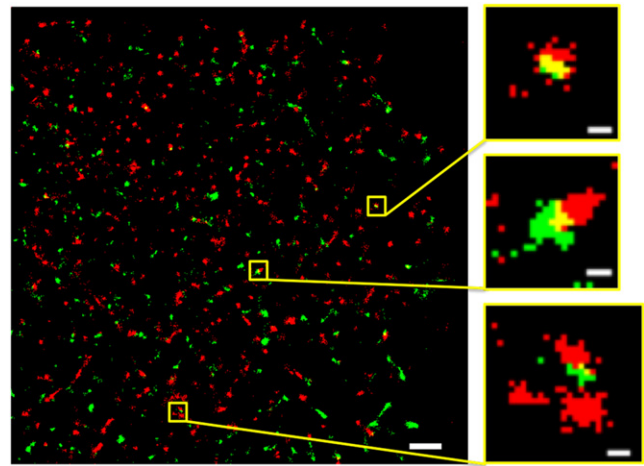
FIGURE 6 DC-SIGN and CD206 plasma membrane nanodomains are usually spatially distinct. Overlay image of DC-SIGN (*green*) and CD206 (*red*) expression on a dendritic cell stained with DCN46, anti-mouse Alexa546, AF2534, and anti-goat ATTO655-Fab using two-color Blink. Regions in yellow boxes are shown at higher magnification to the right and show examples of significant overlap (*top*), minor overlap (*middle*), and no overlap (*bottom*); the latter is the most prevalent situation by far. Scale bar, 500 nm; scale bars insets, 100 nm.

DISCUSSION

How certain receptors are laterally organized on the membrane to enable binding to a large variety of potential ligands, and the interactions of these receptors with other membrane proteins and lipids that enable downstream signaling and internalization, remains a significant open question in biology. DC-SIGN, a CTL, forms clusters on the plasma membrane and these clusters subsequently bind to a diverse range of pathogens, ranging in size, surface composition, and infection route (4,5). The specific manner in which DC-SIGN clustering enables the receptor to bind to such pathogens is under active investigation (29–33). In this work, we have investigated the distribution of DC-SIGN and another CTL, CD206, on dendritic cells using a super-resolution imaging technique, Blink, which has a positional precision (FWHM) for a single dye on glass of ~40 nm. For reference, Blink was also used to image HA expressed on murine fibroblasts.

Blink indicates that DC-SIGN and CD206 are organized into ~80 nm nanodomains on the surface of dendritic cells that cannot be resolved by wide-field fluorescence microscopic methods. Thus, super-resolution (34,35) and ultrastructural methods (5) are required to reveal this unexpected substructure. Interestingly, the viral influenza HA protein, which forms dynamic clusters on the plasma membrane during viral budding, is also organized in ~80 nm nanodomains on the surface of a stable cell line that ectopically expresses HA. However, the overall lateral distribution of CTLs (DC-SIGN and CD206) and HA nanodomains in the plane of the plasma membrane differs

greatly. In the case of DC-SIGN and CD206, nanodomains are randomly distributed on the cell surface, whereas, in the case of HA, the nanodomains are clustered on length scales up to, and sometimes beyond, 1 μm, consistent with earlier studies (21). Moreover, HA can exchange between its microdomains and the surrounding membrane on a rapid timescale; DC-SIGN does not exchange on timescales over several minutes (9). In the case of HA, which must assemble into domains capable of enclosing virions of ~100 nm in diameter, the propensity to cluster and to be expressed in a specific lipid environment may be selecting for a nonrandom distribution of clusters across the cell surface.

Furthermore, because Blink is based upon the sequential localizations of single dyes used for immunofluorescent labeling, it is possible to estimate the occupancy of DC-SIGN in nanodomains. This calculation is accomplished by dividing the number of Blink localizations per nanodomain by the average number of Blink localizations for a single Fab. This analysis estimates that a DC-SIGN nanodomain contains on average, and as a lower bound, 1–3 tetramers, suggesting both that DC-SIGN is not densely packed within nanodomains (Fig. 7) and that other proteins and lipids occupy such nanodomains. Thus, in the absence of ligand, DC-SIGN receptors are organized to have a 4- to 12- fold increased valency, at a minimum, compared to a single receptor. This multivalency, in combination with the extreme lateral stability of the microdomains (8,9), may allow the nanodomains to more effectively interact with weakly binding antigen. Interestingly, it has been proposed that only a single HIV-1 Env (envelope glycoprotein) trimer is capable of initiating viral entry (36). Furthermore, two-color Blink determined that microdomains that appear by wide-field microscopy to contain multiple CTLs are composed of discrete nanodomains containing only one type of CTL that are positioned close to one another.

Our results raise a number of important questions for the manner in which DC-SIGN and other CTLs carry out their biological function, and also provide, to our knowledge, new information that will be useful for understanding the relationship between composition, structure, and dynamics for other clusters of plasma membrane receptors in cell biology. First, will the disposition of some membrane proteins (e.g., DC-SIGN and CD206) into elemental nanodomains prove to be a paradigm for certain classes of receptors? Second, what other components reside in the DC-SIGN and CD206 nanodomains and how are these nanodomains stabilized? For DC-SIGN, these questions are particularly intriguing because microdomain stability appears not to depend directly on the presence of the cytoplasmic domain but rather on the ectodomain of the protein (9,37). Third, from an immunological point of view, how does the distribution of DC-SIGN nanodomains adjust to accommodate large and small pathogens with different glycan patterns on their surfaces? Answers to these questions will substantially increase our understanding of membrane domain structures, their relation to function and, in the case of DC-SIGN and other CTLs, perhaps provide clues for the design of new therapeutic agents for human infectious diseases.

SUPPORTING MATERIAL

REFERENCES

1. Banchereau, J., and R. M. Steinman. 1998. Dendritic cells and the control of immunity. *Nature.* 392:245–252.

2. Altfeld, M., L. Fadda, …, N. Bhardwaj. 2011. DCs and NK cells: critical effectors in the immune response to HIV-1. *Nat. Rev. Immunol.* 11:176–186.

3. Cambi, A., M. Koopman, and C. G. Figdor. 2005. How C-type lectins detect pathogens. *Cell. Microbiol.* 7:481–488.

4. Svajger, U., M. Anderluh, …, N. Obermajer. 2010. C-type lectin DC-SIGN: an adhesion, signalling and antigen-uptake molecule that guides dendritic cells in immunity. *Cell. Signal.* 22:1397–1405.

5. Cambi, A., F. de Lange, …, C. G. Figdor. 2004. Microdomains of the C-type lectin DC-SIGN are portals for virus entry into dendritic cells. *J. Cell Biol.* 164:145–155.

Close-packed Tetramers **Lower Estimate of Number of Tetramers in a Nanodomain**

~76 nm   ~76 nm

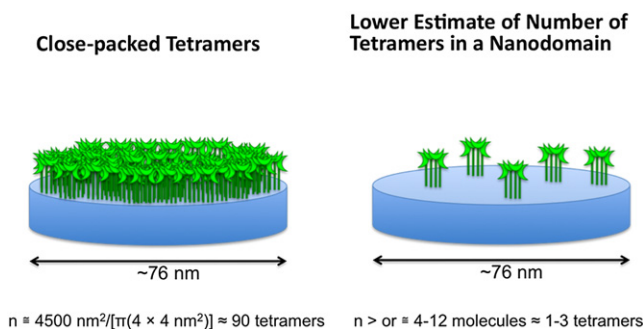n ≈ 4500 nm²/[π(4 × 4 nm²)] ≈ 90 tetramers   n > or ≈ 4-12 molecules ≈ 1-3 tetramers

FIGURE 7 Model of occupancy of DC-SIGN in single nanodomains. A schematic depicting the distribution of DC-SIGN tetramers in a single DC-SIGN nanodomain on a dendritic cell. If the entire area of ~76 nm in diameter nanodomain was occupied by DC-SIGN tetramers (~8 nm in diameter (27,28)), one would expect ~90 tetramers to be in a single nanodomain. However, data using the super-resolution Blink imaging method indicates that, as a lower limit, as few as 1–3 tetramers occupy a single DC-SIGN domain, leaving room for many other receptors and lipids to co-occupy the nanodomains.

6. de Bakker, B. I., F. de Lange, …, M. F. Garcia-Parajo. 2007. Nanoscale organization of the pathogen receptor DC-SIGN mapped by single-molecule high-resolution fluorescence microscopy. *Chem. Phys. Chem.* 8:1473–1480.

7. Koopman, M., A. Cambi, …, M. F. Garcia-Parajo. 2004. Near-field scanning optical microscopy in liquid for high resolution single molecule detection on dendritic cells. *FEBS Lett.* 573:6–10.

8. Neumann, A. K., N. L. Thompson, and K. Jacobson. 2008. Distribution and lateral mobility of DC-SIGN on immature dendritic cells—implications for pathogen uptake. *J. Cell Sci.* 121:634–643.

9. Itano, M. S., A. K. Neumann, …, K. Jacobson. 2011. DC-SIGN and influenza hemagglutinin dynamics in plasma membrane microdomains are markedly different. *Biophys. J.* 100:2662–2670.

10. Mitchell, D. A., A. J. Fadden, and K. Drickamer. 2001. A novel mechanism of carbohydrate recognition by the C-type lectins DC-SIGN and DC-SIGNR. Subunit organization and binding to multivalent ligands. *J. Biol. Chem.* 276:28939–28945.

11. Curtis, B. M., S. Scharnowske, and A. J. Watson. 1992. Sequence and expression of a membrane-associated C-type lectin that exhibits CD4-independent binding of human immunodeficiency virus envelope glycoprotein gp120. *Proc. Natl. Acad. Sci. USA.* 89:8356–8360.

12. Soilleux, E. J., R. Barten, and J. Trowsdale. 2000. DC-SIGN; a related gene, DC-SIGNR; and CD23 form a cluster on 19p13. *J. Immunol.* 165:2937–2942.

13. Su, S. V., P. Hong, …, B. Lee. 2004. DC-SIGN binds to HIV-1 glycoprotein 120 in a distinct but overlapping fashion compared with ICAM-2 and ICAM-3. *J. Biol. Chem.* 279:19122–19132.

14. Feinberg, H., Y. Guo, …, W. I. Weis. 2005. Extended neck regions stabilize tetramers of the receptors DC-SIGN and DC-SIGNR. *J. Biol. Chem.* 280:1327–1335.

15. Serrano-Gómez, D., E. Sierra-Filardi, …, A. L. Corbí. 2008. Structural requirements for multimerization of the pathogen receptor dendritic cell-specific ICAM3-grabbing non-integrin (CD209) on the cell surface. *J. Biol. Chem.* 283:3889–3903.

16. Yu, Q. D., A. P. Oldring, …, M. E. Taylor. 2009. Autonomous tetramerization domains in the glycan-binding receptors DC-SIGN and DC-SIGNR. *J. Mol. Biol.* 387:1075–1080.

17. Steinhauer, C., C. Forthmann, …, P. Tinnefeld. 2008. Superresolution microscopy on the basis of engineered dark states. *J. Am. Chem. Soc.* 130:16840–16841.

18. Leser, G. P., and R. A. Lamb. 2005. Influenza virus assembly and budding in raft-derived microdomains: a quantitative analysis of the surface distribution of HA, NA and M2 proteins. *Virology.* 342:215–227.

19. Takeda, M., G. P. Leser, …, R. A. Lamb. 2003. Influenza virus hemagglutinin concentrates in lipid raft microdomains for efficient viral fusion. *Proc. Natl. Acad. Sci. USA.* 100:14610–14617.

20. Vogelsang, J., C. Steinhauer, …, P. Tinnefeld. 2010. Make them blink: probes for super-resolution microscopy. *Chem. Phys. Chem.* 11:2475–2490.

21. Hess, S. T., T. J. Gould, …, J. Zimmerberg. 2007. Dynamic clustered distribution of hemagglutinin resolved at 40 nm in living cell membranes discriminates between raft theories. *Proc. Natl. Acad. Sci. USA.* 104:17370–17375.

22. Hess, S. T., M. Kumar, …, J. Zimmerberg. 2005. Quantitative electron microscopy and fluorescence spectroscopy of the membrane distribution of influenza hemagglutinin. *J. Cell Biol.* 169:965–976.

23. Gamblin, S. J., and J. J. Skehel. 2010. Influenza hemagglutinin and neuraminidase membrane glycoproteins. *J. Biol. Chem.* 285:28403–28409.

24. Thompson, R. E., D. R. Larson, and W. W. Webb. 2002. Precise nanometer localization analysis for individual fluorescent probes. *Biophys. J.* 82:2775–2783.

25. Hammer, Ø., D. A. T. Harper, and P. D. Ryan. 2001. PAST: paleontological statistics software package for education and data analysis. *Palaeon. Electron.* 4:1–9.

26. Zhang, J., K. Leiderman, …, S. L. Steinberg. 2006. Characterizing the topography of membrane receptors and signaling molecules from spatial patterns obtained using nanometer-scale electron-dense probes and electron microscopy. *Micron.* 37:14–34.

27. Guo, Y., H. Feinberg, …, K. Drickamer. 2004. Structural basis for distinct ligand-binding and targeting properties of the receptors DC-SIGN and DC-SIGNR. *Nat. Struct. Mol. Biol.* 11:591–598.

28. Feinberg, H., D. A. Mitchell, …, W. I. Weis. 2001. Structural basis for selective recognition of oligosaccharides by DC-SIGN and DC-SIGNR. *Science.* 294:2163–2166.

29. Menon, S., K. Rosenberg, …, D. E. Leckband. 2009. Binding-site geometry and flexibility in DC-SIGN demonstrated with surface force measurements. *Proc. Natl. Acad. Sci. USA.* 106:11524–11529.

30. Hodges, A., K. Sharrocks, …, A. Simmons. 2007. Activation of the lectin DC-SIGN induces an immature dendritic cell phenotype triggering Rho-GTPase activity required for HIV-1 replication. *Nat. Immunol.* 8:569–577.

31. Gringhuis, S. I., J. den Dunnen, …, T. B. Geijtenbeek. 2007. C-type lectin DC-SIGN modulates Toll-like receptor signaling via Raf-1 kinase-dependent acetylation of transcription factor NF-kappaB. *Immunity.* 26:605–616.

32. Cambi, A., D. S. Lidke, …, T. M. Jovin. 2007. Ligand-conjugated quantum dots monitor antigen uptake and processing by dendritic cells. *Nano Lett.* 7:970–977.

33. Avota, E., E. Gulbins, and S. Schneider-Schaulies. 2011. DC-SIGN mediated sphingomyelinase-activation and ceramide generation is essential for enhancement of viral uptake in dendritic cells. *PLoS Pathog.* 7:e1001290.

34. Betzig, E., G. H. Patterson, …, H. F. Hess. 2006. Imaging intracellular fluorescent proteins at nanometer resolution. *Science.* 313:1642–1645.

35. Hell, S. W. 2009. Microscopy and its focal switch. *Nat. Methods.* 6:24–32.

36. Yang, X., S. Kurteva, …, J. Sodroski. 2005. Stoichiometry of envelope glycoprotein trimers in the entry of human immunodeficiency virus type 1. *J. Virol.* 79:12132–12147.

37. Liu, P., X. Wang, …, N. L. Thompson. 2012. The formation and stability of DC-SIGN microdomains require its extracellular moiety. *Traffic.* 10.1111/j.1600-0854.2012.01337.x. In press. [Epub ahead of print].

38. Baribaud, F., S. Pöhlmann, …, R. W. Doms. 2001. Functional and antigenic characterization of human, rhesus macaque, pigtailed macaque, and murine DC-SIGN. *J. Virol.* 75:10281–10289.

39. Braciale, T. J., M. E. Andrew, and V. L. Braciale. 1981. Simultaneous expression of H-2-restricted and alloreactive recognition by a cloned line of influenza virus-specific cytotoxic T lymphocytes. *J. Exp. Med.* 153:1371–1376.

40. Vogelsang, J., T. Cordes, …, P. Tinnefeld. 2009. Controlling the fluorescence of ordinary oxazine dyes for single-molecule switching and superresolution microscopy. *Proc. Natl. Acad. Sci. USA.* 106:8107–8112.

41. Steinhauer, C., R. Jungmann, …, P. Tinnefeld. 2009. DNA origami as a nanoscopic ruler for super-resolution microscopy. *Angew. Chem. Int. Ed. Engl.* 48:8870–8873.